

Optimization of communication topology for persistent formation in case of communication faults

Guo-Qiang Wang(王国强), He Luo(罗贺), Xiao-Xuan Hu(胡笑旋), and Jian-Wei Tai(台建玮)
Citation: Chin. Phys. B, 2023, 32 (**7**): 078901. DOI: 10.1088/1674-1056/acb0c0
Journal homepage: http://cpb.iphy.ac.cn; http://iopscience.iop.org/cpb

What follows is a list of articles you may be interested in

A novel similarity measure for mining missing links in long-path networks

Yijun Ran(冉义军), Tianyu Liu(刘天宇), Tao Jia(贾韬), and Xiao-Ke Xu(许小可)
Chin. Phys. B, 2022, 31 (**6**): 068902. DOI: 10.1088/1674-1056/ac4483

Uncovering offline event similarity of online friends by constructing null models

Wenkuo Cui(崔文阔), Jing Xiao(肖婧), Ting Li(李婷), Xiaoke Xu(许小可)
Chin. Phys. B, 2019, 28 (**6**): 068901. DOI: 10.1088/1674-1056/28/6/068901

Controllability of heterogeneous interdependent group systems under undirected and directed topology

Hui-Qin Pei(裴惠琴), Shi-Ming Chen(陈世明)
Chin. Phys. B, 2018, 27 (**10**): 108901. DOI: 10.1088/1674-1056/27/10/108901

Generation of optimal persistent formations for heterogeneous multi-agent systems with a leader constraint

Guo-Qiang Wang(王国强), He Luo(罗贺), Xiao-Xuan Hu(胡笑旋)
Chin. Phys. B, 2018, 27 (**2**): 028901. DOI: 10.1088/1674-1056/27/2/028901

Constrained consensuses in disconnected topologies

Song Hai-Yu(宋海裕), Yu Li(俞立), Hu Hong-Xiang(胡鸿翔), and Zhang Wen-An(张文安)
Chin. Phys. B, 2012, 21 (**2**): 028901. DOI: 10.1088/1674-1056/21/2/028901

Optimization of communication topology for persistent formation in case of communication faults

Guo-Qiang Wang(王国强)[1,2,3], He Luo(罗贺)[1,2,3,†], Xiao-Xuan Hu(胡笑旋)[1,2,3], and Jian-Wei Tai(台建玮)[1,2,3]

[1] *School of Management, Hefei University of Technology, Hefei* 230009, *China*
[2] *Key Laboratory of Process Optimization & Intelligent Decision-making, Ministry of Education, Hefei* 230009, *China*
[3] *Engineering Research Center for Intelligent Decision-making & Information Systems Technologies, Ministry of Education, Hefei* 230009, *China*

(Received 24 September 2022; revised manuscript received 5 December 2022; accepted manuscript online 6 January 2023)

To address the optimization problem of communication topology for persistent formation in the case of communication faults such as link interruption, transmitter failure, and receiver failure a two-stage model including fast reconstruction of communication topology and re-optimization of communication topology is constructed. Then, a fast reconstruction algorithm of communication topology for persistent formation (FRA-CT-PF), based on optimally rigid graph, arc addition operation, and path reversal operation, is proposed, which can quickly generate a feasible reconstructed communication topology after communication faults, thus ensuring the safety of the agents and maintaining the formation shape of persistent formation. Furthermore, a re-optimization algorithm of communication topology for persistent formation (ROA-CT-PF), based on agent position exchange, is proposed, which can further obtain a reoptimized communication topology to minimize the formation communication cost while still maintaining the formation shape of persistent formation. The time complexities of these two algorithms are also analyzed. Finally, the effectiveness of the above algorithms is verified by numerical experiments. Compared with existing algorithms, FRA-CT-PF can always obtain feasible reconstructed communication topology in much less time under all communication fault scenarios, and ROA-CT-PF can obtain a reoptimized communication topology to further reduce the formation communication cost in a shorter time.

Keywords: persistent formation, communication topology, formation communication cost, communication fault

PACS: 89.20.Ff, 87.85.St, 02.10.Ox, 64.60.aq **DOI:** 10.1088/1674-1056/acb0c0

1. Introduction

Agent formation has been widely used in many fields, such as large-object transportation,[1] mobile target tracking,[2] and earth observing.[3] To maintain the formation shape, there are mainly the following three formation control methods: position-based,[4,5] displacement-based,[6,7] and distance-based[8,9] methods. In comparison with other methods, the distance-based method has the advantage of requiring no knowledge of the orientations of the agents in global coordinates.[10] Agent formation using distance-based method can be further divided into two categories: rigid formation[11,12] and persistent formation.[13,14] Compared with the rigid formation, the persistent formation only needs to use half of the communication links.[15]

In a persistent formation, one agent usually acts as the leader and tracks a predetermined reference trajectory, and the other agents receive the information from some of their neighboring agents through communication links to keep the distances between them constant. All the available communication links and the communication links being used to maintain the formation shape constitute the network topology and communication topology of the persistent formation respectively.[16] To ensure that the persistent formation can maintain its formation shape, the communication topology must be a persistent graph of the network topology. Meanwhile, different communication links of each agent may have different communication costs, that is, they consume different energy of the agent, and the available energy of each agent is limited, so it is necessary to optimize the communication topology of a persistent formation to minimize the energy consumption of the agents.

With the aim of minimizing the sum of the communication costs of all communication links in the communication topology, also called the formation communication cost, the concept of a min-weighted persistent formation[17] or an optimally persistent formation[18] has been proposed. To generate the communication topology of an optimally persistent formation, a generation algorithm based on optimally rigid graph and triangular configuration has been proposed,[17] which is suitable for a specific two-dimensional (2D) formation shape. Two generation algorithms based on optimally rigid graph and several oriented operations have been proposed,[19,20] which are suitable for any 2D and three-dimensional (3D) formation shape respectively. In addition, a generation algorithm based on optimally rigid graph with a top–down strategy has been proposed,[21] which can be applied to some 3D formation shapes.

Furthermore, considering the leader constraint (only cer-

[†]Corresponding author. E-mail: luohe@hfut.edu.cn

© 2023 Chinese Physical Society and IOP Publishing Ltd

tain agents can act as the leader of the formation), two algorithms called LC-HMAS-OPFGA[16] and CTOA-3DPF-LC,[22] based on optimally rigid graph, minimum cost arborescence (MCA), and path reversal operation, have been proposed, which are suitable for any 2D and 3D formation shapes respectively. Then, two corresponding improved algorithms with less calculation time, called FOA-CT-2DPF[23] and FGA-CT-3DOPF,[24] have also been proposed.

In summary, the existing studies have mainly addressed the offline optimization problem of communication topology for persistent formation without communication faults. However, owing to hostile attacks, signal jamming or occlusion, mechanical or communication hardware failure and so on, a persistent formation may suffer communication faults during formation movement. These communication faults may cause some communication links in the current communication topology to no longer be usable or some agents to withdraw from the formation.[25] As a result, the formation shape cannot be maintained, and agent collisions may even occur in serious cases. Therefore, it is necessary to optimize the communication topology after such communication faults to ensure the safety of all agents and continue to maintain the formation shape while reducing the formation communication cost as much as possible. Therefore, studied in this work is the optimization problem of communication topology for persistent formation in case of communication faults, and the main novel contributions of this paper are as follows.

(i) A two-stage optimization model is proposed, which decomposes this problem into two simpler subproblems, that is, the fast reconstruction subproblem of communication topology and the re-optimization subproblem of communication topology.

(ii) For the first subproblem, a fast reconstruction algorithm of communication topology, based on optimally rigid graph, arc addition operation and path reversal operation, is proposed, which can ensure the safety of the agents in a timely manner and maintain the formation shape.

(iii) For the second subproblem, a re-optimization algorithm of communication topology, based on agent position exchange, is proposed, which can ensure that the formation communication cost is as low as possible while still maintaining the formation shape.

The remainder of this article is organized as follows. The problem analysis and modeling are discussed in Section 2. In Section 3, the proposed algorithms are presented in detail, and their time complexities are analyzed. In Section 4, the effectiveness of the proposed algorithms is validated by numerical experiments. Concluding remarks and expectations are presented in Section 5.

2. Problem analysis and modeling

First, some basic knowledge about persistent formation is presented. Second, the communication fault constraint of a persistent formation is analyzed. On this basis, a two-stage optimization model is proposed to model the optimization problem of communication topology for persistent formation in case of communication faults.

2.1. Basic knowledge about persistent formation

The formation shape, network topology, communication topology, leader constraint, and communication fault constraint of persistent formation are introduced respectively.

2.1.1. Formation shape of persistent formation

The d-dimensional formation shape of a persistent formation composed of n agents can be represented by an $n\times 3$ matrix $\boldsymbol{S}$,[23,24] as shown below:

$$\boldsymbol{S}=\begin{bmatrix}(x_1,y_1,z_1)\\ \cdots\\ (x_i,y_i,z_i)\\ \cdots\\ (x_n,y_n,z_n)\end{bmatrix}. \tag{1}$$

Here, the positions in the formation shape are numbered as $1,2,\ldots,n$, and (x_i,y_i,z_i) represent the relative coordinates of the i-th position in a coordinate system. In particular, when d is equal to 2, the value of z_i $(1\le i\le n)$ is 0.

2.1.2. Network topology of persistent formation

The network topology of a persistent formation includes all of the available communication links between agents, and can be represented by a weighted digraph $D=(V,A,W,P)$ as follows.[23,24]

i) $V=\{v_i\},1\le i\le n$, is the set of vertices, where v_i represents the i-th agent.

ii) $A=\{a_{ij}\}\subset V\times V,1\le i\ne j\le n$, is the set of arcs, where $a_{ij}=(v_i,v_j)$ denotes that there is a communication link from v_i to v_j such that v_i can send information to v_j.

iii) $W=\{w_{ij}\},a_{ij}\in A$, is the set of arc weights, where w_{ij} denotes the communication cost of a_{ij}, which is equivalent to the communication distance from v_i to v_j.

iv) $P=\{p_i\},1\le i\le n$, is the set of specific positions of agents, referred to as the agent position configuration, where p_i represents the number of the specific position of v_i in $\boldsymbol{S}$.

2.1.3. Communication topology of persistent formation

The communication topology of a persistent formation is a persistent graph in its network topology. It can be expressed as $T=(V,A^*,W^*,P),A^*\subseteq A,W^*\subseteq W$, and has the following attributes.[23,24]

(I) Its underlying undirected graph is a rigid graph.

(II) $a_{ij} \in A^*$ indicates that the communication link from v_i to v_j is used during the formation movement.

(III) $d_T^-(v_i)$ denotes the in-degree of v_i in T, which must satisfy $d_T^-(v_i) \leq d$.

(IV) $|A^*|$ represents the total number of communication links in the communication topology, which must satisfy $|A^*| \geq d \times (|V|-3)+3$. When $|A^*| = d \times (|V|-3)+3$, the communication topology is a minimally persistent graph, and the persistent formation is a minimally persistent formation.

(V) $w(T) = \sum_{a_{ij} \in A^*} w_{ij}$ represents the formation communication cost. If the corresponding $w(T)$ of the current communication topology is the smallest in all possible persistent graphs in the same network topology, then this communication topology is an optimally persistent graph, and this formation is an optimally persistent formation.

2.1.4. Leader constraint of persistent formation

To facilitate agent control, the leader-first-follower (LFF) or leader-remote-follower (LRF) control mode is usually used by a persistent formation to maintain a 2D formation shape. Furthermore, for a heterogeneous persistent formation, only specific agents can act as the leader in the LFF or LRF control mode, and these candidate leaders can be represented by $V^l \subseteq V$. Therefore, the leader constraint of a 2D persistent formation can be described as Eq. (2),[23] in which v_i acts as the leader.

$$\exists (v_i \in V^l) : d_T^-(v_i) = 0. \tag{2}$$

Similarly, the leader-first follower-second follower (L-FF-SF) control mode is usually used by a persistent formation to maintain a 3D formation shape, and the leader constraint of a 3D persistent formation can be described as follows:[24]

$$\begin{aligned} &\exists (v_i \in V^l) : a_{ij} \in A^*,\ \ a_{ik} \in A^*,\ \ a_{jk} \in A^*, \\ &d_T^-(v_i) = 0,\ \ d_T^-(v_j) = 1,\ \ d_T^-(v_k) = 2, \end{aligned} \tag{3}$$

where v_i, v_j, and v_k act as the leader, the first follower, and the second follower, respectively.

2.2. Communication fault constraint of persistent formation

Four specific types of communication faults can be summarized in Table 1.[26]

Table 1. Four types of communication faults.

Type	Description
Link interruption	when a_{ij} suffers a link interruption, v_j cannot receive any information that v_i sends through a_{ij}; however, both the transmitter of v_i and the receiver of v_j are functioning.
Transmitter failure	when v_i suffers a transmitter failure, v_i cannot send any information to other agents.
Receiver failure	when v_i suffers a receiver failure, v_i cannot receive any information from other agents.
Transceiver failure	when v_i suffers a transceiver failure, v_i can neither send any information to other agents nor receive any information from other agents. In this case, v_i must withdraw from the formation.

Meanwhile, for all agents to be informed of the same communication fault information in time, we assume that all agents have the same diagnosis and identification strategy of communication faults based on a broadcast communication channel (BC) as indicated in the studies of Giulietti *et al.*,[27] Pollini *et al.*,[28] and Yang *et al.*[29]

In summary, different types of communication faults will make certain communication links invalid or cause certain agents to withdraw from the formation. Let $A^- = \{a_{xy}\}$, $1 \leq x \neq y \leq n$, represent the set of invalid communication links, and let $V^- = \{a_z\}$, $1 \leq z \leq n$, denote the set of agents that must be withdrawn from the formation. If the current communication topology contains one or more of these invalid communication links or if one or more of the agents need to be withdrawn from the formation, then the current communication topology can no longer be used to maintain the formation shape, and the communication topology must be adjusted. Therefore, the communication fault constraint of a persistent formation can be described as follows:

$$A^* \cap A^- = \Phi \quad \text{and} \quad V \cap V^- = \Phi. \tag{4}$$

That is, the adjusted communication topology cannot contain any invalid communication links, nor can it contain any agent that needs to withdraw from the formation.

2.3. Problem modeling

When a communication fault prevents the current communication topology from being used to maintain the formation shape, if the communication topology is not adjusted in time, this communication fault may lead to collision accidents between agents.[25] Therefore, after a communication fault occurs, the communication topology must be quickly reconstructed to ensure the safety of the agents and restore the formation shape. After the communication topology reconstruction, the security of the persistent formation is ensured. At this time, the communication topology can be reoptimized via agent position exchange (*e.g.*, exchanging the positions of two agents in the formation or having one agent filling in the space left by another agent exiting the formation) to achieve the minimal formation communication cost required to continue to maintain the formation shape. Based on the above

analysis, the optimization problem of communication topology for persistent formation in case of communication faults can be decomposed into the following two subproblems.

I) Fast reconstruction subproblem of communication topology for persistent formation

First, the corresponding invalid arcs or invalid vertices are removed from the current network topology $D=(V,A,W,P)$ to obtain a reconstructed network topology $D_{\rm r}=(V_{\rm r},A_{\rm r},W_{\rm r},P_{\rm r})$ that satisfies the communication fault constraint; then, a suitable subgraph $T_{\rm r}$ needs to be quickly selected from $D_{\rm r}$ as the reconstructed communication topology.

The reconstructed communication topology must be a persistent graph in $D_{\rm r}$; however, there may be more than one graph like this in $D_{\rm r}$, of which, the optimally persistent graph has the lowest formation communication cost. Moreover, because only certain agents can serve as the leader, it may not be possible to use any arbitrary optimally persistent graph in $D_{\rm r}$ as the reconstructed communication topology. Therefore, this problem is modeled as an optimization problem of obtaining the optimally persistent graph in $D_{\rm r}$ that satisfies the leader constraint and the communication fault constraint.

II) Re-optimization subproblem of communication topology for persistent formation

Since different position exchanges will result in different agent position configurations $P_{\rm m}$ and there are multiple feasible communication topologies for each $P_{\rm m}$, in this work this problem is modeled as a combinatorial optimization problem in which the leader constraint and the communication fault constraint must be satisfied: the objective is to select an optimal position configuration $P_{\rm o}$ from the set of all possible agent position configurations $\{P_{\rm m}\}$ such that the formation communication cost of the corresponding optimal communication topology $T_{\rm o}$ is globally minimum.

Specifically, the network topology $D_{\rm m}$ that satisfies the communication fault constraint is constructed for each $P_{\rm m}$, and then, the optimally persistent graph $T_{\rm m}$ that satisfies the leader constraint in $D_{\rm m}$ is obtained. Finally, the graph with the lowest formation communication cost is selected as the reoptimized communication topology $T_{\rm o}$ from among all $T_{\rm m}$, and the corresponding agent position configuration $P_{\rm o}$ is the reoptimized agent position configuration.

The necessary and sufficient conditions for an optimally persistent graph are shown in Lemma 1 as follows.

Lemma 1[16,22] A weighted digraph $D=(V,A,W)$ is a d-dimensional optimally persistent graph if and only if it satisfies the following two conditions:

(i) The in-degree of each vertex is no greater than d.

(ii) The corresponding weighted undirected graph, $G=(V,E,W)$, is a d-dimensional optimally rigid graph.

The necessary and sufficient conditions for an optimally rigid graph, as mentioned in condition 2 of Lemma 1, are shown in Lemma 2 as follows.

Lemma 2[16,22] A weighted undirected graph $G=(V,E,W)$ is a d-dimensional optimally rigid graph if and only if it satisfies the following three conditions:

i) The number of edges, $|E|$, is $d\times(|V|-3)+3$.

ii) The corresponding rigidity matrix, $\boldsymbol{M}\in\boldsymbol{R}^{|E|\times(3\times|V|)}$, is full rank, that is, the rank of $\boldsymbol{M}$ is $d\times(|V|-3)+3$.

iii) The sum of the weights of all edges in E is the smallest in all weighted undirected graphs that have the same vertices and satisfy conditions 1 and 2.

3. Model-solving algorithms

For solving the above two subproblems, a fast reconstruction algorithm of communication topology for persistent formation (FRA-CT-PF), based on optimally rigid graph, arc addition operation and path reversal operation, is proposed. Then, a re-optimization algorithm of communication topology for persistent formation (ROA-CT-PF), based on agent position exchange, is proposed. The details of these two algorithms are described in the following subsections.

3.1. FRA-CT-PF

The algorithm first deletes invalid arcs and vertexes from current network topology to obtain a reconstructed network topology, then generates an optimally rigid graph of this reconstructed network topology by considering the communication fault constraint, and transforms the optimally rigid graph into an optimally persistent graph satisfying the communication fault constraint through converting into a digraph, obtaining the intersection with current communication topology, arc addition and path reversal operations. Finally, the algorithm makes the optimally persistent graph satisfy both the leader constraint and the communication fault constraint through path reversal operation. The pseudocode of FRA-CT-PF is shown in Table 2.

Next, the correctness of FRA-CT-PF is proved theoretically.

Theorem 1 The reconstructed communication topology $T_{\rm r}$ obtained by FRA-CT-PF must be the optimally persistent graph in the reconstructed network topology $D_{\rm r}$ that satisfies the leader constraint and the communication fault constraint.

Proof Because T is a d-dimensional optimally persistent graph of D, the in-degree of each vertex in T is no greater than d according to Lemma 1. Therefore, after the operation of line 09, the in-degree of each vertex in $T_{\rm r}$ is also no greater than d. The premise of the operation of line 15 is $d^-_{T_{\rm r}}(v_j)<d$, which ensures that $d^-_{T_{\rm r}}(v_j)\le d$ and the in-degrees of other vertices do not change after this operation. Because $d^-_{T_{\rm r}}(v_j)=d$ before

the operation of line 19, $d^-_{T_r}(v_j) = d+1$ holds after the arc addition operation in line 19. Then, line 19 finds a path from v_k satisfying $d^-_{T_r}(v_k) < d$ to v_j and line 20 reverses this path. After this path reversal operation, $d^-_{T_r}(v_j) = d$, $d^-_{T_r}(v_k) \leq d$, and the in-degrees of other vertices do not change. Similarly, after the operations in lines 17, 22, and 23, the in-degree of each vertex in T_r must be no greater than d. After the operations in lines 11 to 27, $m = d \times (|V_r| - 3) + 3$. Meanwhile, the operations in lines 28 to 36 can also ensure that in-degree of each vertex in T_r must also be no greater than d. That is, T_r obtained by FRA-CT-PF must satisfy condition 1 of Lemma 1.

After the operation of line 08, D_{Rr} is the digraph of optimally rigid graph R_r. After the operation of line 09, T_r is a subgraph of D_{Rr} and no duplicate arcs exist in T_r. In the operations of lines 11 to 27, all arcs added to T_r must belong to D_{Rr} and no duplicate arcs are added to T_r. Meanwhile, after the operations of lines 11 to 27, $m = d \times (|V_r| - 3) + 3$. In the operations of lines 28 to 36, only the direction of some arcs in T_r is changed. Therefore, the corresponding weighted undirected graph of the final T_r must be the optimally rigid graph R_r. That is, T_r obtained by FRA-CT-PF must satisfy condition 2 of Lemma 1.

Because all conditions of Lemma 1 are satisfied, T_r obtained by FRA-CT-PF must be a d-dimensional optimally persistent graph in D_r.

After the operation of lines 28 to 36, $d = 2$ and equation (2) are satisfied, or $d = 3$ and equation (3) are satisfied. Therefore, T_r obtained by FRA-CT-PF must satisfy the leader constraint.

Table 2. Pseudocode of FRA-CT-PF.

Algorithm 1: FRA-CT-PF

Input: $\boldsymbol{S}$: formation shape; d: dimension of formation shape; $D = (V, A, W, P)$: current network topology; $T = (V, A^*, W^*, P)$: current communication topology; $A^- = \{a_{xy}\}, 1 \leq x \neq y \leq |V|$: set of invalid communication links; $V^- = \{a_z\}, 1 \leq z \leq n$: set of agents that need to withdraw from the formation; V^l: set of candidate leaders;

Output: $D_r = (V_r, A_r, W_r, P_r)$: reconstructed network topology; $T_r = (V_r, A^*_r, W^*_r, P_r)$: reconstructed communication topology;

01: **Initialize** $D_r = D$ and $T_r = T$;
02: Delete A^- and V^- from D_r; // After this operation, D_r is the reconstructed network topology
03: **if** $A^*_r \cap A^- = \emptyset$ **and** $V_r \cap V^- = \emptyset$ **then**
04: **return**; // The current communication topology is not affected by the communication fault
05: **end if**
06: Convert the arcs in D_r into edges and obtain an undirected graph G_r;
07: Generate an optimally rigid graph R_r of G_r, which satisfies that the degree of each vertex in R_r is no more than the number of bidirectional arcs of this vertex in G_r plus d;
08: Convert each edge in R_r into one arc or two arcs to obtain a digraph D_{Rr}, which satisfies $D_{Rr} \subseteq D_r$;
09: $T_r = D_{Rr} \cap T$;
10: Get the number of arcs, m, in T_r;
11: **while** $m < d \times (|V_r| - 3) + 3$ **do**
12: $l = 1$
13: **if** (neither a_{ij} nor a_{ji}, which corresponds to the l-th edge e_{ij} in R_r, exists in T_r) **then**
14: **if** $d^-_{T_r}(v_j) < d$ and $a_{ij} \in D_{Rr}$ **then**
15: Add a_{ij} to T_r, and let $m = m + 1$;
16: **else if** $d^-_{T_r}(v_i) < d$ and $a_{ji} \in D_{Rr}$ **then**
17: Add a_{ji} to T_r, and let $m = m + 1$;
18: **else if** $a_{ij} \in D_{Rr}$ **then**
19: Add a_{ij} to T_r, and find v_k which satisfies $d^-_{T_r}(v_k) < d$, has a path to v_j in T_r and its reverse path exists in D_{Rr};
20: Reverse all arcs of this path in T_r, and let $m = m + 1$;
21: **else if** $a_{ji} \in D_{Rr}$ **then**
22: Add a_{ji} to T_r, and find v_k which satisfies $d^-_{T_r}(v_k) < d$, has a path to v_i in T_r and its reverse path exists in D_{Rr};
23: Reverse all arcs of this path in T_r, and let $m = m + 1$;
24: **end if**
25: **end if**
26: $l = l + 1$
27: **end while**
28: **if** ($d = 2$ and equation (2) is satisfied) || ($d = 3$ and equation (3) is satisfied) **then**
29: **return**; //T_r satisfies the leader constraint, so it is the reconstructed communication topology
30: **else**
31: Find v_i in T_r that satisfies $v_i \in V^l$, and perform path reverse operations in T_r until $d^-_{T_r}(v_i) = 0$ and $T_r \subseteq D_{Rr}$;
32: **if** $d = 3$ **then**
33: Find v_j in T_r that satisfies $a_{ij} \in A^*_r$, and perform path reverse operations in T_r until $d^-_{T_r}(v_j) = 1$ and $T_r \subseteq D_{Rr}$;
34: Find v_k in T_r that satisfies $a_{ik}, a_{jk} \in A^*_r$, and perform path reverse operations in T_r until $d^-_{T_r}(v_k) = 2$ and $T_r \subseteq D_{Rr}$;
35: **end if**
36: **end if**
37: **return**; //T_r is the reconstructed communication topology

After the operation of line 03, A^- and V^- are deleted from D_r, which means that D_r satisfies the communication fault constraint. After the operations of lines 08 to 09, D_{Rr} is the subgraph of D_r and T_r is the subgraph of D_{Rr}, so T_r satisfies the communication fault constraint. In the operations of lines 11 to 36, all arcs added to T_r must belong to D_{Rr} and all the reverse paths must exist in D_{Rr}. Therefore, T_r obtained by FRA-CT-PF must satisfy the communication fault constraint.

In summary, T_r obtained by FRA-CT-PF must be the optimally persistent graph in D_r that satisfies the leader constraint and the communication fault constraint.

The time complexity of FRA-CT-PF is analyzed as follows. In this algorithm, the main calculation time is in lines 07, 19, 22, 31, 33, and 34, respectively. Line 07 is an improvement on the original optimally rigid graph generation algorithm,[30] and its time complexity is approximately $O(|V_r|^4)$. Lines 19, 22, 31, 33, and 34 use the classical Dijkstra shortest path algorithm, and the time complexity of each of them is approximately $O(|A_r^*|+|V_r|\times\log|V_r|)$. Because $|V_r|\le|V|$ and $|A_r^*|\le|A_r|\le|V|\times(|V|-1)$, the total time complexity of FRA-CT-PF is about $O(|V_r|^4+4\times(|A_r^*|+|V_r|\times\log|V_r|))\approx O(|V|^4)$.

3.2. ROA-CT-PF

To obtain a reoptimized communication topology through agent position exchange, the following solution method can be adopted. First, for each agent position configuration P_m, the network topology D_m that satisfies the communication fault constraint is constructed. Then, the optimally persistent graph T_m that satisfies the leader constraint and the communication fault constraint in each D_m, is obtained. Finally, the graph with the lowest formation communication cost is selected from among all T_m as the reoptimized communication topology, T_o.

However, each P_m must be a permutation of the selection of $|V_r|$ positions from among the $|V|$ positions in the formation shape, so the total number of all possible P_m is $|V|!/(|V|-|V_r|)!$. As the value of $|V|$ continues to increase, the corresponding value of $|V|!/(|V|-|V_r|)!$ becomes very large, indicating that it is difficult to obtain a solution in a limited time. Therefore, ROA-CT-PF is proposed in this work to achieve a suboptimal reoptimized communication topology through position exchange between only two agents. Nevertheless, it can still obtain a good reoptimized communication topology, as verified in the following numerical experiments. The pseudocode of this algorithm is shown in Table 3.

Table 3. Pseudocode of ROA-CT-PF.

Algorithm 2: ROA-CT-PF

Input: S: formation shape; d: dimension of formation shape; $T=(V,A^*,W^*,P)$: current communication topology; $D_r=(V_r,A_r,W_r,P_r)$: reconstructed network topology; $T_r=(V_r,A_r^*,W_r^*,P_r)$: reconstructed communication topology; V^l: set of candidate leaders;

Output: $T_o=(V_r,A_o^*,W_o^*,P_o)$: reoptimized communication topology;

01: **Initialize** $m=1$, $P_m=P_r$ and $T_o=T_r$, where $P_o=P_r$;

02: **if** $|V_r|=|V|$ and $w(T_o)=w(T)$ **then**

03: **return**; // The reconstructed communication topology is simply the reoptimized communication topology

04: **end if**

05: **while** $m<|V|\times(|V|-1)/2$ **do**

06: Let $m=m+1$, and obtain the next untested combination $\{i,j\}$ of 2 elements selected from $\{1,2,.,|V|\}$; then, let $P_m=P_r$, exchange the values of p_i and p_j in P_m to obtain the new agent position configuration P_m;

07: Construct the corresponding network topology $D_m=(V_r,A_m,W_m,P_m)$ for P_m that satisfies the communication fault constraint;

08: Based on D_m and V^l, refer to lines 06 to 36 of Algorithm 1 to obtain the corresponding optimal reconstructed communication topology $T_m=(V_r,A_m^*,W_m^*,P_m)$;

09: **if** $w(T_m)<w(T_o)$ **then**

10: Let $T_o=T_m$, where $P_o=P_m$;

11: **else if** ($w(T_m)=w(T_o)$ and the total agent movement distance for switching from P_r to P_m is less than that to P_o) **then**

12: Let $T_o=T_m$, where $P_o=P_m$;

13: **end if**

14: **end while**

15: **return**; //T_o is the reoptimized communication topology

Next, the correctness of ROA-CT-PF is proved theoretically.

Theorem 2 The reoptimized communication topology T_o obtained by ROA-CT-PF must be feasible and its formation communication cost is no more than that of T_r obtained by FRA-CT-PF.

Proof In the operation of line 01, T_o is initialized by the reconstructed communication topology T_r obtained by FRA-CT-PF. According to Theorem 1, T_r must be feasible, so the initial T_o is feasible. In the operation of line 08, FRA-CT-PF is used to obtain the corresponding optimal reconstructed communication topology T_m. According to Theorem 1, T_m must be feasible. In the operations of lines 10 and 12, T_o is replaced by T_m. Therefore, T_o obtained by ROA-CT-PF must be feasible.

In the operation of line 01, T_o is initialized by the reconstructed communication topology T_r obtained by FRA-CT-PF, so the formation communication cost of the initial T_o is equal to that of T_r. In the operations of lines 09 to 13, only when $w(T_m) \leq w(T_o)$ T_o can be replaced by T_m. Therefore, the formation communication cost of T_o obtained by ROA-CT-PF is no more than that of T_r obtained by FRA-CT-PF.

The time complexity of ROA-CT-PF is analyzed as follows. Line 08 is the core step of this algorithm and is the same as lines 06 to 36 of FRA-CT-PF; therefore, the time complexity of line 08 is approximately $O(|V|^4)$. In line 06 the number of possible combinations of two positions selected from among the $|V|$ total positions is $|V| \times (|V|-1)/2$; that is, the total number of all feasible P_m is $|V| \times (|V|-1)/2$. Therefore, it can be seen from line 05 of this algorithm that line 08 will run $|V| \times (|V|-1)/2$ times at most. Consequently, because $|V_r| \leq |V|$, the time complexity of this algorithm is approximately $O(|V|^4 \times |V| \times (|V|-1)/2) \approx O(|V|^6)$.

4. Numerical experiments

Next, several numerical experiments are carried out to verify the effectiveness of the proposed algorithms.

4.1. Experimental settings

Consider a persistent formation consisting of six agents that need to maintain the 3D formation shape shown in Fig. 1.

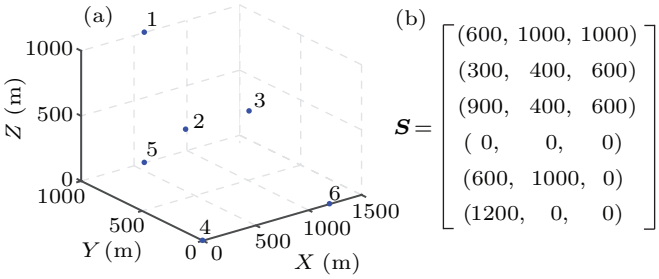


Fig. 1. Formation shape of persistent formation consisting of six agents, showing (a) relative spatial locations of all positions and (b) relative coordinates of all positions.

Assuming that there are no communication faults at the beginning, all agents are able to communicate with each other, v_i is located at the i-th position in $\boldsymbol{S}$ and only v_1, v_2, and v_4 can serve as leaders, so the initial network topology is shown in Fig. 2(a) and its corresponding Laplace matrix is

$$L_D = \begin{bmatrix} 5 & -781.025 & -781.025 & -1536.23 & -1000 & -1536.23 \\ -781.025 & 5 & -600 & -781.025 & -900 & -1153.26 \\ -781.025 & -600 & 5 & -1153.26 & -900 & -781.025 \\ -1536.23 & -781.025 & -1153.26 & 5 & -1166.19 & -1200 \\ -1000 & -900 & -900 & -1166.19 & 5 & -1166.19 \\ -1536.23 & -1153.26 & -781.025 & -1200 & -1166.19 & 5 \end{bmatrix}.$$

The initial communication topology of this persistent formation, obtained by CTOA-PF-LC,[22] is shown in Fig. 2(b). Its corresponding Laplace matrix is

$$L_T = \begin{bmatrix} 0 & -781.025 & -781.025 & 0 & -1000 & 0 \\ 0 & 1 & -600 & -781.025 & -900 & -1153.26 \\ 0 & 0 & 3 & -1153.26 & 0 & -781.025 \\ 0 & 0 & 0 & 3 & 0 & 0 \\ 0 & 0 & -900 & -1166.19 & 2 & -1166.19 \\ 0 & 0 & 0 & 0 & 0 & 3 \end{bmatrix}.$$

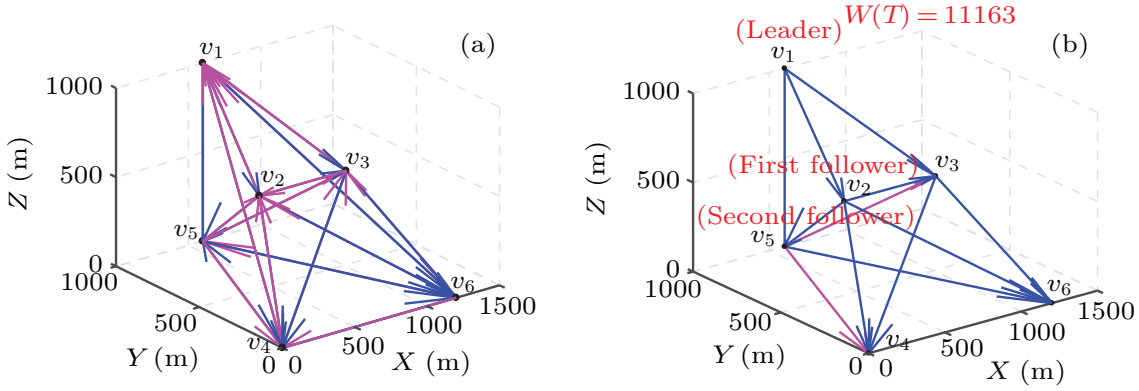


Fig. 2. Initial network topology and communication topology of this persistent formation, showing (a) initial network topology and (b) initial communication topology.

Table 4. Eight communication fault scenarios.

Scenario	Type of communication fault	Specific contents of communication fault
Scenario 1	link interruption	a_{13}, a_{45}, and a_{54} suffer link interruption
Scenario 2	transmitter failure	v_1 suffers a transmitter failure
Scenario 3	transmitter failure	v_5 suffers a transmitter failure
Scenario 4	receiver failure	v_4 suffers a receiver failure
Scenario 5	transceiver failure	v_1 suffers a transceiver failure
Scenario 6	transceiver failure	v_3 suffers a transceiver failure
Scenario 7	transceiver failure	v_1 and v_6 suffer a transceiver failure
Scenario 8	transceiver failure	v_2 and v_5 suffer a transceiver failure

In this communication topology, v_1, v_2, and v_5 are the leader, the first follower, and the second follower, respectively, and the formation communication cost is 11163, while $P = \{1,2,3,4,5\}$ is the corresponding agent position configuration. To easily distinguish the in-degree of each vertex in figures, arcs from small- to large-numbered vertices are drawn with blue solid lines, and other arcs are drawn with magenta solid lines.

To verify the effectiveness of proposed algorithms under various types of communication faults in Table 1, eight communication fault scenarios as shown in Table 4, are designed and the corresponding numerical experiments are carried out. Among these scenarios, because the influence of a transmitter or transceiver failure on a leader in the communication topology is very different from that of a transmitter or transceiver failure on a non-leader, scenarios 2 and 3 are designed to represent transmitter failures on a leader and a non-leader, and scenarios 5 and 6 are designed to represent transceiver failures on a leader and a non-leader, respectively. In addition, scenarios 7 and 8 are designed to represent transceiver failures on two agents.

The development environment of all algorithms is Visual Studio 2013, and the programming language is C++. All experiments are performed on a computer with an 8-core i7 4.0-GHz processor, 16-GB RAM and a Windows 10 operating system.

4.2. Experimental results of fast reconstruction of communication topology

First, scenario 3 is used to illustrate the calculation process of FRA-CT-PF. It is assumed that v_5 suffers a transmitter failure based on the current network topology shown in Fig. 2(a) and the current communication topology shown in Fig. 2(b). At the same time, only v_1, v_2, and v_4 can serve as leaders. Namely, the communication fault constraint is denoted by $A^- = \{a_{5y}\}, 1 \le y \le 6$ and $V^- = \emptyset$, and the leader constraint is represented by $V^l = \{v_1, v_2, v_4\}$. Then, the main calculation process of this algorithm is as follows.

In line 02, the invalid arcs and vertexes are deleted from current network topology, and the reconstructed network topology D_r is shown in Fig. 3(a). Its corresponding Laplace matrix is

$$L_{D_r} = \begin{bmatrix} 4 & -781.025 & -781.025 & -1536.23 & -1000 & -1536.23 \\ -781.025 & 4 & -600 & -781.025 & -900 & -1153.26 \\ -781.025 & -600 & 4 & -1153.26 & -900 & -781.025 \\ -1536.23 & -781.025 & -1153.26 & 4 & -1166.19 & -1200 \\ 0 & 0 & 0 & 0 & 5 & 0 \\ -1536.23 & -1153.26 & -781.025 & -1200 & -1166.19 & 4 \end{bmatrix}.$$

In line 07, the optimally rigid graph R_r of G_r is generated as shown in Fig. 3(b), which satisfies that the degree of each vertex in R_r is no more than the number of bidirectional arcs of this vertex in G_r plus 3. This additional condition ensures that R_r can be directed to an optimally persistent graph satisfying the communication fault constraint.

In line 08, R_r is converted into a digraph D_{Rr} satisfying the communication fault constraint, and it is shown in Fig. 3(c). Its corresponding Laplace matrix is

$$L_{D_{Rr}} = \begin{bmatrix} 4 & -781.025 & -781.025 & -1536.23 & -1000 & -1536.23 \\ -781.025 & 4 & -600 & -781.025 & -900 & -1153.26 \\ -781.025 & -600 & 4 & -1153.26 & -900 & -781.025 \\ -1536.23 & -781.025 & -1153.26 & 3 & 0 & 0 \\ 0 & 0 & 0 & 0 & 3 & 0 \\ -1536.23 & -1153.26 & -781.025 & 0 & 0 & 3 \end{bmatrix}.$$

In line 09, the intersection of D_{Rr} and T is obtained and used to reinitialize T_r, as shown in Fig. 3(d).

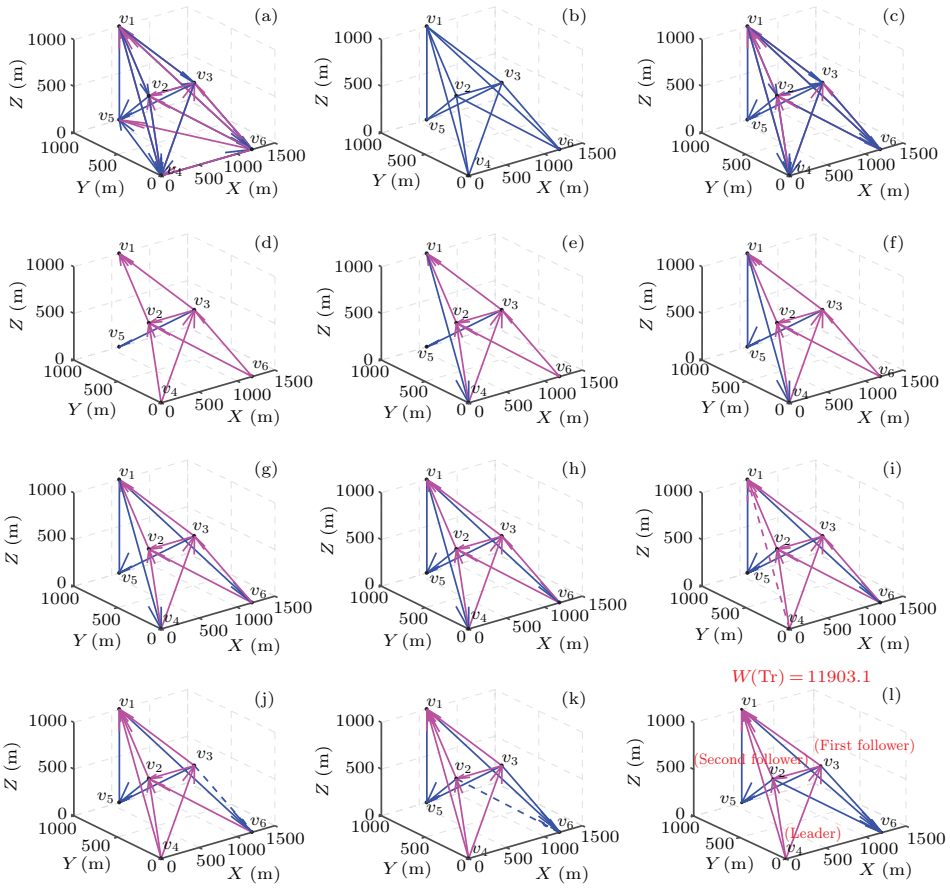


Fig. 3. Calculation process of FRA-CT-PF under scenario 3, showing (a) constructed network topology, (b) optimally rigid graph R_r, (c) digraph corresponding to R_r, (d) intersection T_r of D_Rr and T, (e) T_r after adding a_{14}, (f) T_r after adding a_{15}, (g) T_r after adding a_{16}, (h) T_r after adding a_{25}, (i) T_r after reversing $(1,4)$, (j) T_r after reversing $(6,3)$, (k) T_r after reversing $(6,2)$, and (l) reconstructed communication topology.

In line 10, the number of its arcs, m, is 8.

In line 11, because $m < 3\times|V_\mathrm{r}|-6$, the operations in lines 12 to 26 will be performed until $m = 3\times|V_\mathrm{r}|-6$. The specific process is as follows: when $l=1$, the l-th edge e_{ij} in R_r is e_{14}, neither a_{14} nor a_{41} exists in T_r, $d^-_{T_\mathrm{r}}(v_4)=0<3$ and $a_{14}\in D_\mathrm{Rr}$, so a_{14} is added to T_r in line 15 as shown in Fig. 3(e). Similarly, when $l=2$, a_{15} is added to T_r as shown in Fig. 3(f). When $l=3$, a_{16} is added to T_r as shown in Fig. 3(g). When $l=4$, a_{25} is added to T_r as shown in Fig. 3(h).

In line 28, because the leader constraint is not satisfied, jumps directly to line 31.

In line 31, v_4 is found to be the leader because it satisfies $v_4\in V^l$. However, because $d^-_{T_\mathrm{r}}(v_4)=1$ now, a path $(1,4)$ is found in T_r and its arcs are reversed in T_r as shown in Fig. 3(i), where the reversed path is identified by dashed lines. After this path reverse operation, T_r satisfies $d^-_{T_\mathrm{r}}(v_4)=0$ and $T_\mathrm{r}\subseteq D_\mathrm{Rr}$. Therefore, v_4 acts as the leader.

In line 33, v_3 is found because it satisfies $a_{43}\in A^*_\mathrm{r}$. However, because $d^-_{T_\mathrm{r}}(v_3)=2$ now, a path $(6,3)$ is found in T_r and its arcs are reversed in T_r as shown in Fig. 3(j), where the reversed path is identified by dashed lines. After this path reverse operation, T_r satisfies $a_{43}\in A^*_\mathrm{r}$, $d^-_{T_\mathrm{r}}(v_3)=1$ and $T_\mathrm{r}\subseteq D_\mathrm{Rr}$. Therefore, v_3 acts as the first follower.

In line 34, v_2 is found because it satisfies $a_{42},a_{32}\in A^*_\mathrm{r}$. However, because $d^-_{T_\mathrm{r}}(v_2)=3$ now, a path $(6,2)$ is found in T_r and its arcs are reversed in T_r as shown in Fig. 3(k), where the reversed path is identified by dashed lines. After this path reverse operation, T_r satisfies $a_{42},a_{32}\in A^*_\mathrm{r}$, $d^-_{T_\mathrm{r}}(v_2)=2$ and $T_\mathrm{r}\subseteq D_\mathrm{Rr}$. Therefore, v_2 acts as the second follower.

In line 37, T_r is the reconstructed communication topology as shown in Fig. 3(l), and the corresponding formation communication cost is 11903.1. Its corresponding Laplace matrix is

$$L_{T_\mathrm{r}}=\begin{bmatrix} 3 & 0 & 0 & 0 & -1000 & -1536.23\\ -781.025 & 2 & 0 & 0 & -900 & -1153.26\\ -781.025 & -600 & 1 & 0 & -900 & -781.025\\ -1536.23 & -781.025 & -1153.26 & 0 & 0 & 0\\ 0 & 0 & 0 & 0 & 3 & 0\\ 0 & 0 & 0 & 0 & 0 & 3 \end{bmatrix}.$$

Comparatively, if CTOA-3DPF-LC[22] is used to acquire the reconstructed communication topology in this case, the final T_r obtained is shown in Fig. 4. However, the arcs a_{53}, a_{54}, and a_{56} exist in the final T_r, which means that the final T_r does not satisfy the communication fault constraint. Therefore, the reconstructed communication topology obtained by CTOA-3DPF-LC is infeasible.

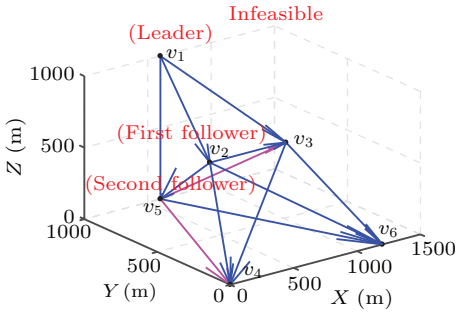


Fig. 4. Reconstructed communication topology obtained by CTOA-3DPF-LC.

Similarly, if FGA-CT-3DOPF[24] is used to obtain the reconstructed communication topology in this case, the final T_r obtained is shown in Fig. 5. However, it does not satisfy the condition 1 of Lemma 2. Therefore, the reconstructed communication topology obtained by FGA-CT-3DOPF is also infeasible.

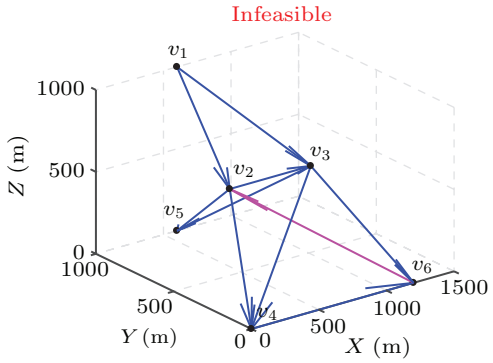


Fig. 5. Reconstructed communication topology obtained by FGA-CT-3DOPF.

Table 5. Reconstructed communication topologies and calculation time under eight scenarios.

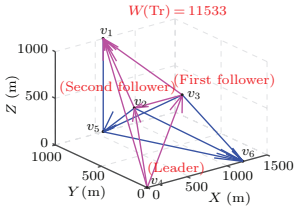
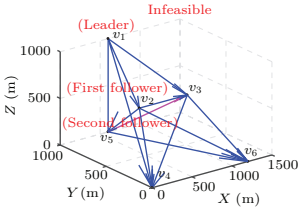
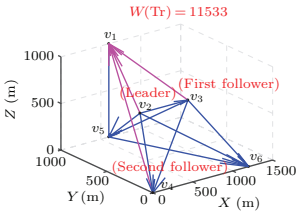
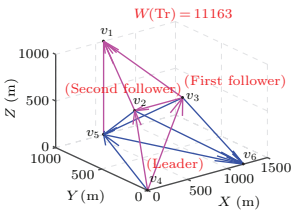
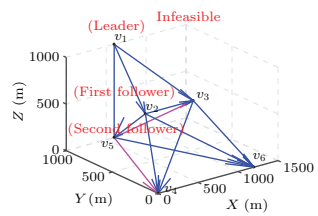
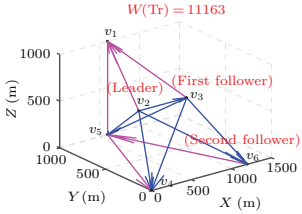
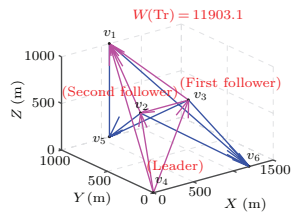
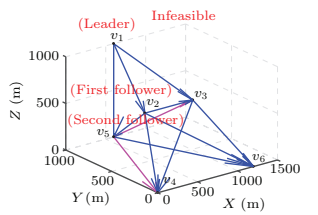
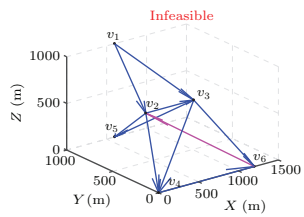
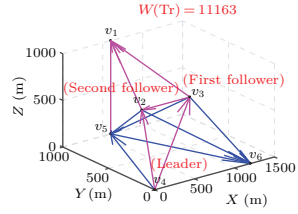
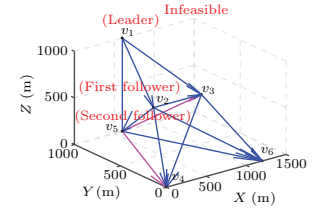
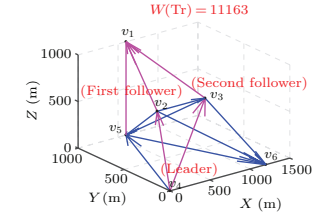
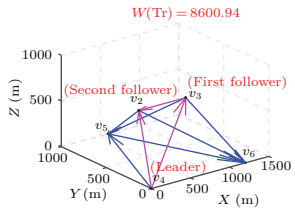
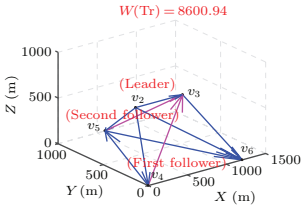
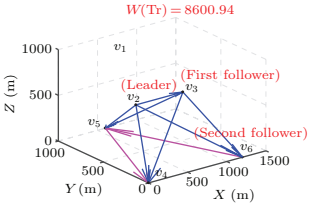
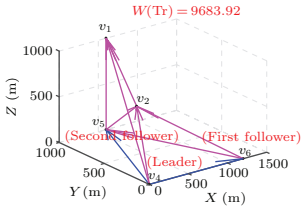
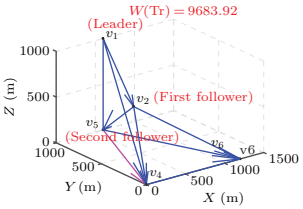
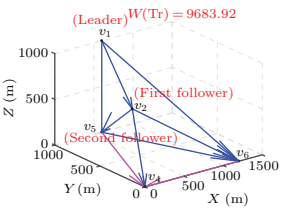
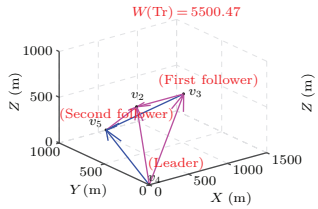
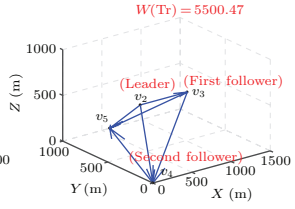
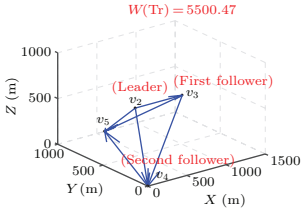
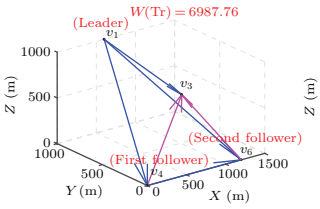
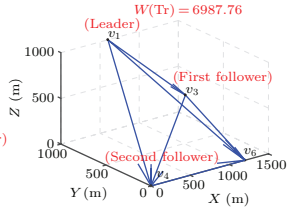
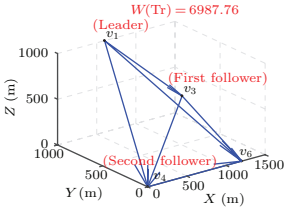
Scenario	FRA-CT-PF	CTOA-3DPF-LC	FGA-CT-3DOPF
Scenario 1: a_{13}, a_{45} and a_{54} suffer link interruption	 0.034 s	 0.616 s	 1.909 s
Scenario 2: v_1 suffers a transmitter failure	 0.032 s	 0.723 s	 1.804 s
Scenario 3: v_5 suffers a transmitter failure	 0.037 s	 0.769 s	 2.093 s
Scenario 4: v_4 suffers a receiver failure	 0.032 s	 0.487 s	 1.775 s

Table 5. (Continued).

Scenario	FRA-CT-PF	CTOA-3DPF-LC	FGA-CT-3DOPF
Scenario 5: v_1 suffers a transceiver failure	 $W(\mathrm{Tr}) = 8600.94$ 0.015 s	 $W(\mathrm{Tr}) = 8600.94$ 0.604 s	 $W(\mathrm{Tr}) = 8600.94$ 1.862 s
Scenario 6: v_3 suffers a transceiver failure	 $W(\mathrm{Tr}) = 9683.92$ 0.015 s	 $W(\mathrm{Tr}) = 9683.92$ 0.703 s	 $W(\mathrm{Tr}) = 9683.92$ 2.933 s
Scenario 7: v_1 and v_6 suffer a transceiver failure	 $W(\mathrm{Tr}) = 5500.47$ 0.007 s	 $W(\mathrm{Tr}) = 5500.47$ 0.542 s	 $W(\mathrm{Tr}) = 5500.47$ 2.819 s
Scenario 8: v_2 and v_5 suffer a transceiver failure	 $W(\mathrm{Tr}) = 6987.76$ 0.007 s	 $W(\mathrm{Tr}) = 6987.76$ 0.696 s	 $W(\mathrm{Tr}) = 6987.76$ 2.319 s

Next, for the eight communication fault scenarios in Table 4, the reconstructed communication topologies obtained by FRA-CT-PF and existing algorithms, and the calculation time of these algorithms are shown in Table 5.

In scenario 1, the reconstructed communication topologies obtained by FRA-CT-PF and FGA-CT-3DOPF are both feasible and have the same formation communication cost. However, the reconstructed communication topology obtained by CTOA-3DPF-LC is infeasible because it does not satisfy the communication fault constraint. In scenarios 2 and 4, the same conclusion can be drawn.

In scenario 3, the reconstructed communication topology obtained by FRA-CT-PF is feasible. However, the reconstructed communication topology obtained by CTOA-3DPF-LC is infeasible because it does not satisfy the communication fault constraint. Meanwhile, the reconstructed communication topology obtained by FGA-CT-3DOPF is infeasible because it does not satisfy the condition 1 of Lemma 2.

In scenario 5, the reconstructed communication topologies obtained by FRA-CT-PF, CTOA-3DPF-LC and FGA-CT-3DOPF are both feasible and have the same formation communication cost. In scenarios 6, 7, and 8, the same conclusion can be drawn.

Meanwhile, in all scenarios, the average calculation time of FRA-CT-PF is only 3.48% of that of CTOA-3DPF-LC, but only 1.02% of that of FGA-CT-3DOPF.

In summary, compared with existing algorithms, FRA-CT-PF proposed in this paper can always obtain feasible reconstructed communication topology in all communication fault scenarios, and its calculation time is much less.

4.3. Experimental results of re-optimization of communication topology

First, scenario 3 continues to be used to illustrate the calculation process of ROA-CT-PF. Based on the reconstructed communication topology as shown in Fig. 3(l), the calculation

process of ROA-CT-PF is as follows.

In line 01, T_o is equal to T_r and P_o is equal to P_r.

In line 02, because $w(T_o) = 11903.1$ and $w(T) = 11163$, the algorithm executes the operations of lines 05 to 14.

When $m = 2$, the corresponding P_2 in line 06 is $\{2,1,3,4,5,6\}$ and the corresponding T_2 in line 08 is shown in Fig. 6(a), where v_1 and v_2 exchange their positions in the formation shape and $w(T_2) = 11903.1$. Because $w(T_2) = w(T_o)$ and the total agent movement distance for switching from P_r to P_2 is 1562.05, which is more than that from P_r to P_o, there is no change in T_o nor P_o.

When $m = 3$, P_3 is $\{3,2,1,4,5,6\}$ and T_3 is shown in Fig. 6(b), where v_1 and v_3 exchange their positions in the formation shape and $w(T_3) = 11903.1$. Because $w(T_3) = w(T_o)$ and the total agent movement distance for switching from P_r to P_3 is equal to that from P_r to P_o, there is no change in T_o and P_o, either.

When $m = 4$, P_4 is $\{4,2,3,1,5,6\}$ and T_4 is shown in Fig. 6(c), where v_1 and v_4 exchange their positions in the formation shape and $w(T_4) = 11903.1$. Because $w(T_4) = w(T_o)$ and the total agent movement distance for switching from P_r to P_4 is 3072.46, which is more than that from P_r to P_o, there is also no change in T_o nor P_o.

When $m = 5$, P_5 is $\{5,2,3,4,1,6\}$ and T_5 is shown in Fig. 6(d), where v_1 and v_5 exchange their positions in the formation shape and $w(T_5) = 11163$. Because $w(T_5) < w(T_o)$, the operation of line 10 is executed, which means $T_o = T_5$ and $P_o = P_5$.

From $m = 6$ to the end, the conditions in line 09 or line 11 are not satisfied, so there is no change in T_o nor P_o. Namely, T_5 is the reoptimized communication topology, where v_1 and v_5 exchange their positions.

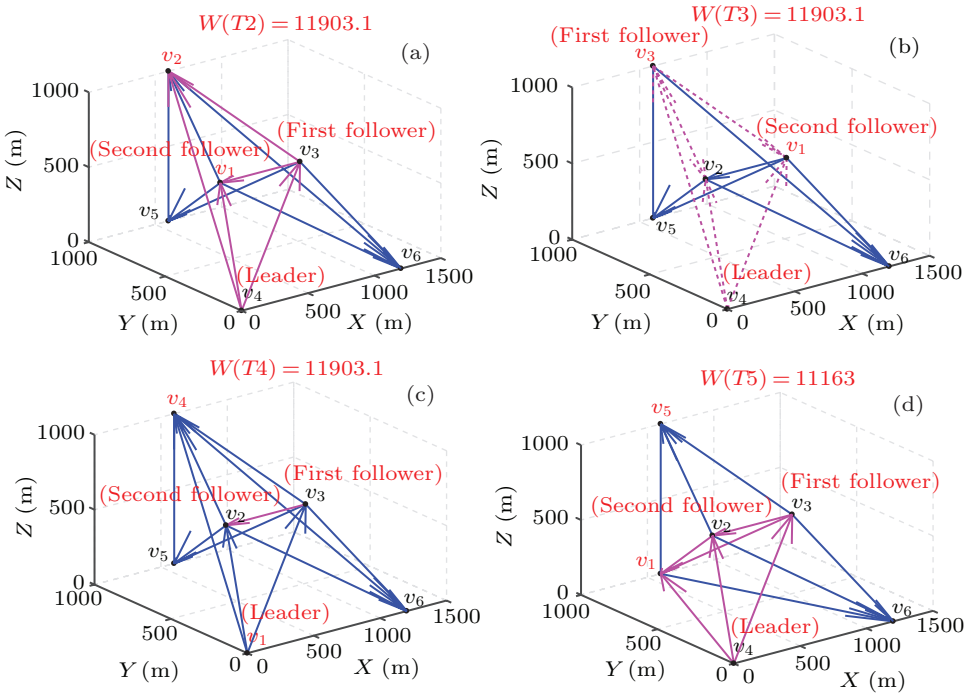


Fig. 6. Example of calculation process of ROA-CT-PF, showing: (a) reconstructed communication topology when $m = 2$, (b) reconstructed communication topology when $m = 3$, (c) reconstructed communication topology when $m = 4$, and (d) reoptimized communication topology.

In contrast, lines 05 and 06 of ROA-CT-PF are modified into "while $m < |V|!/(|V| - |V_r|)!$ do" and "Let $m = m+1$, and obtain the next permutation P_m of the selection of $|V_r|$ positions from among the $|V|$ positions in the formation shape", and this modified algorithm is called ROA-CT-PF-P. Then, ROA-CT-PF-P is used to obtain the reoptimized communication topology in this case. The T_o obtained by ROA-CT-PF-P is the same as that obtained by ROA-CT-PF, but the calculation time of ROA-CT-PF-P is much longer than that of ROA-CT-PF.

Next, for the eight communication fault scenarios in Table 4, the reoptimized communication topologies obtained by FRA-CT-PF and existing algorithms, and the calculation time of these algorithms are shown in Table 6.

In scenario 1, because the formation communication cost of reconstructed communication topology is more than that of current communication topology, the operations of agent position exchange in ROA-CT-PF and ROA-CT-PF-P will be executed. The reoptimized communication topologies obtained by ROA-CT-PF and ROA-CT-PF-P are the same. However, the calculation time of ROA-CT-PF is much less than that of ROA-CT-PF-P. Meanwhile, both CTOA-3DPF-LC and FGA-CT-3DOPF do not support the re-optimization of communication topology for persistent formation. In scenarios 3, 5, 6, and 7, the same conclusion can be drawn.

In scenario 2, because the formation communication cost of reconstructed communication topology is equal to that of current communication topology, the operations of agent position exchange in ROA-CT-PF and ROA-CT-PF-P will not be executed. That is, the reoptimized communication topologies obtained by ROA-CT-PF and ROA-CT-PF-P are the same as the reconstructed communication topology, and the calculation time of ROA-CT-PF and ROA-CT-PF-P are both approximately equal to 0. In scenario 4, the same conclusion can be drawn.

Table 6. Reoptimized communication topologies and calculation time under eight scenarios

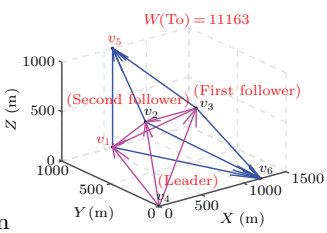
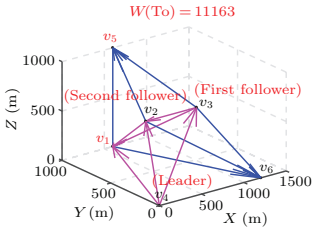
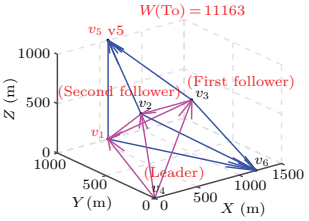
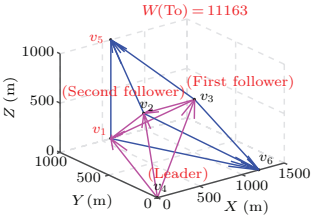
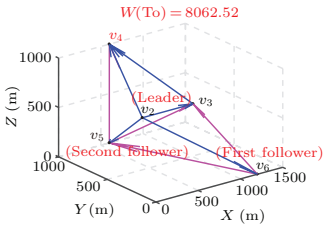
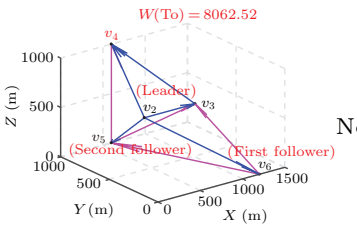
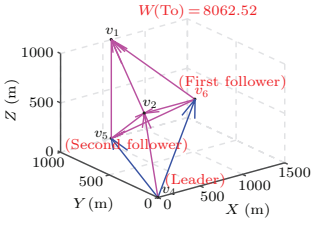
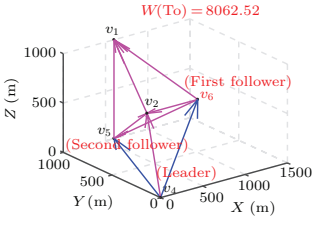
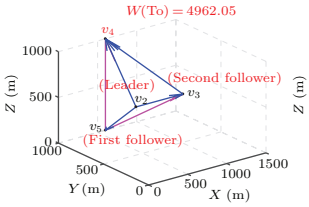
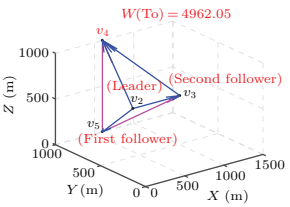
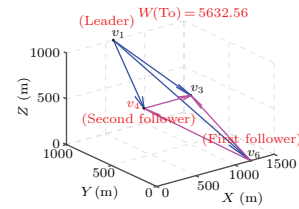
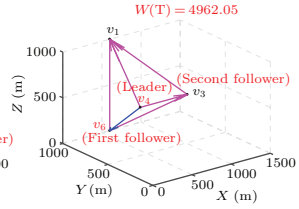
Scenario	ROA-CT-PF	ROA-CT-PF-P	CTOA-3DPF-LC	FGA-CT-3DOPF
Scenario 1: a_{13}, a_{45} and a_{54} suffer link interruption	 0.497 s	 26.333 s	No support	No support
Scenario 2: v_1 suffers a transmitter failure	No change 0 s	No change 0 s	No support	No support
Scenario 3: v_5 suffers a transmitter failure	 0.498 s	 27.489 s	No support	No support
Scenario 4: v_4 suffers a receiver failure	No change 0 s	No change 0 s	No support	No support
Scenario 5: v_1 suffers a transceiver failure	 0.196 s	 10.677 s	No support	No support
Scenario 6: v_3 suffers a transceiver failure	 0.210 s	 10.102 s	No support	No support

Table 6. (Continued).

Scenario	ROA-CT-PF	ROA-CT-PF-P	CTOA-3DPF-LC	FGA-CT-3DOPF
Scenario 7: v_1 and v_6 suffer a transceiver failure	 0.080 s	 3.514 s	No support	No support
Scenario 8: v_2 and v_5 suffer a transceiver failure	 0.090 s	 3.444 s	No support	No support

In scenario 8, because the formation communication cost of reconstructed communication topology is more than that of current communication topology, the operations of agent position exchange in ROA-CT-PF and ROA-CT-PF-P will be executed. The formation communication cost of the reoptimized communication topology obtained by ROA-CT-PF is more than that by ROA-CT-PF-P. This shows that ROA-CT-PF cannot ensure obtaining the optimal reoptimized communication topology through position exchange between only two agents. However, the calculation time of ROA-CT-PF is much less than that of ROA-CT-PF-P.

In summary, the following conclusions can be drawn from Table 6:

(i) Compared with CTOA-3DPF-LC and FGA-CT-3DOPF, the ROA-CT-PF proposed in this paper can reoptimize the communication topology to further reduce the formation communication cost based on the reconstructed communication topology.

(ii) Compared with ROA-CT-PF-P, the ROA-CT-PF proposed in this paper can almost obtain the same reoptimized communication topology in all communication fault scenarios, and the calculation time is much less.

5. Conclusion and perspectives

In this paper, the optimization problem of communication topology for persistent formation in case of communication faults is studied. This problem is decomposed into two subproblems, namely, the fast reconstruction subproblem of communication topology and the re-optimization subproblem of communication topology.

To address the fast reconstruction subproblem of communication topology, an algorithm called FRA-CT-PF, based on optimally rigid graph, arc addition operation and path reversal operation, is proposed. Compared with existing algorithms, the algorithm can always obtain feasible reconstructed communication topology in all communication fault scenarios, and its calculation time is much less.

To address the re-optimization subproblem of communication topology, an algorithm called ROA-CT-PF, based on agent position exchange, is proposed. Compared with existing algorithms, the algorithm can obtain a reoptimized communication topology to further reduce the formation communication cost in a shorter time.

In the future, a distributed optimization algorithm of communication topology for persistent formation in case of communication faults will be studied.

Acknowledgements

Project supported by the National Natural Science Foundation of China (Grant Nos. 71871079, 72271076, 71971075, and 71671059) and the Anhui Provincial Natural Science Foundation, China (Grant No. 1808085MG213).

References

[1] Dai Y Y, Kim Y G, Wee S G, Lee D H and Lee S G 2016 *ISA Transactions* **60** 321
[2] Dutta R, Sun L and Pack D 2018 *IEEE T. Contr. Syst. T.* **26** 2206
[3] Chen Y Y, Yu R, Zhang Y and Liu C L 2020 *IEEE-CAA Journal of Automatica Sinica* **7** 505
[4] Hua C C, Chen J N and Li Y F 2017 *International Journal of Systems Science* **48** 2499
[5] Qian Z L, Lyu W C, Dai Y Z and Xu J 2022 *J. Intell. Robot. Syst.* **106** 15

[6] Dimarogonas D V and Kyriakopoulos K J 2008 *Automatica* **44** 2648
[7] Lin Z Y, Broucke M and Francis B 2004 *IEEE T. Automat Contr.* **49** 622
[8] Summers T H, Yu C B, Dasgupta S and Anderson B D O 2011 *IEEE T. Automat. Contr.* **56** 2772
[9] Liu H, Lin Z, Cao M, Wang X and Lu J 2018 *Systems & Control Letters* **119** 8
[10] Oh K K, Park M C and Ahn H S 2015 *Automatica* **53** 424
[11] Sun Z Y, de Marina H G, Anderson B D O and Cao M 2018 *Int. J. Robust. Nonlin.* **28** 4865
[12] Wu H J, Yang Z H, Cao J N and Lai L Q 2020 *IEEE T. Veh. Technol.* **69** 7679
[13] Kang S M, Park M C and Ahn H S 2017 *IEEE T. Ind. Electron.* **64** 380
[14] Yu D X, Chen C L P, Ren C E and Sui S 2020 *IEEE Transactions on Cybernetics* **50** 4481
[15] Park M C, Jeong K and Ahn H S 2015 *Int. J. Robust & Nonlinear Control* **25** 2532
[16] Wang G Q, Luo H and Hu X X 2018 *Chin. Phys. B* **27** 028901
[17] Luo X Y, Li S B and Guan X P 2009 *Chin. Phys. B* **18** 3104
[18] Shao S K, Luo X Y, Jin T and Guan X P 2012 2012 24*th Chinese Control and Decision Conference (CCDC)*, 23–25 May, 2012, Taiyuan, China, p. 152
[19] Luo X Y, Yang F, Li S B and Guan X P 2014 *Acta Automatica Sinica* **40** 1311
[20] Wang J R, Luo X Y, Yang F and Guan X P 2015 *Acta Automatica Sinica* **41** 1123
[21] Sun H Y, Song G M, Wei Z and Zhang Y 2018 *International Journal of Aerospace Engineering* **2018**
[22] Wang G Q, Luo H, Hu X X and Yang S L 2021 *Optim. Lett.* **15** 513
[23] Wang G Q, Wu P, Li X D, Cao X and Luo H 2021 2021 *China Automation Congress (CAC)*, 22–24 October, 2021, Beijing, China, p. 1671
[24] Wang G Q, Lv Q W, Li X D, Cao X and Luo H 2021 2021 33*rd Chinese Control and Decision Conference (CCDC)*, 22–24 May, 2021, Kunming, China, p. 3193
[25] Motevallian S A, Yu C B and Anderson B D O 2015 *Int. J. Robust. Nonlin.* **25** 1654
[26] Wang G Q, Luo H, Hu X X, Ma H W and Yang S L 2017 *Int. J. Adv. Robot. Syst.* **14** 1
[27] Giulietti F, Pollini L and Innocenti M 2000 *IEEE Control Systems* **20** 34
[28] Pollini L, Giulietti F and Innocenti M 2002 *American Control Conference*, May 8–10,2002, Hilton Anchorage and Egan Convention Center, Anchorage, Alaska, USA, p. 2860
[29] Yang H, Jiang B and Zhang Y M 2014 *International Journal of Control Automation and Systems* **12** 29
[30] Xue L, Chen X, Zhao J J and Guan X P 2015 2015 34*th Chinese Control Conference (CCC)*, 28–30 July, 2015, Hangzhou, China, p. 7795